Energy and frequency dependence of the alpha particle redistribution produced by internal kink modes

R. Farengo, H. E. Ferrari, P. L. Garcia-Martinez, M.-C. Firpo, W. Ettoumi, and A. F. Lifschitz

Citation: Physics of Plasmas (1994-present) **21**, 082512 (2014); doi: 10.1063/1.4893145
View online: http://dx.doi.org/10.1063/1.4893145
View Table of Contents: http://scitation.aip.org/content/aip/journal/pop/21/8?ver=pdfcov
Published by the AIP Publishing

Energy and frequency dependence of the alpha particle redistribution produced by internal kink modes

R. Farengo,[1] H. E. Ferrari,[1,2] P. L. Garcia-Martinez,[2] M.-C. Firpo,[3] W. Ettoumi,[3] and A. F. Lifschitz[4]
[1]*Comisión Nacional de Energía Atómica, Centro Atómico Bariloche e Instituto Balseiro, 8400 Bariloche, RN, Argentina*
[2]*CONICET, 8400 Bariloche, RN, Argentina*
[3]*Laboratoire de Physique des Plasmas, CNRS, Ecole Polytechnique, 91128, Palaiseau cedex, France*
[4]*Laboratoire d'Optique Appliquee, ENSTA, CNRS, Ecole Polytechnique, 91761 Palaiseau cedex, France*

(Received 30 April 2014; accepted 1 August 2014; published online 15 August 2014)

The redistribution of alpha particles due to internal kink modes is studied. The exact particle trajectories in the total fields, equilibrium plus perturbation, are calculated. The equilibrium has circular cross section and the plasma parameters are similar to those expected in ITER. The alpha particles are initially distributed according to a slowing down distribution function and have energies between 18 keV and 3.5 MeV. The (1, 1), (2, 2), and (2, 1) modes are included and the effect of changing their amplitude and frequency is studied. When only the (1, 1) mode is included, the spreading of high energy ($E \gtrsim 1$ MeV) alpha particles increases slowly with the energy and mode frequency. At lower energies, the redistribution is more sensitive to the mode frequency and particle energy. When a (2, 1) mode is added, the spreading increases significantly and particles can reach the edge of the plasma. Trapped particles are the most affected and the redistribution parameter can have maxima above 1 MeV, depending on the mode frequency. These results can have important implications for ash removal. © *2014 AIP Publishing LLC*.
[http://dx.doi.org/10.1063/1.4893145]

I. INTRODUCTION

The internal kink modes associated with sawtooth oscillations can produce a redistribution of the alpha particle population, thus modifying the power deposition profile and increasing alpha particle losses and wall loading. In addition, alpha particle transport from the core to the outer region can trigger other instabilities. Although the redistribution of high energy alpha particles would reduce reactor performance, the removal of low energy particles (helium ash) is needed to sustain a high fusion power. The ideal situation would therefore be one where the high energy particles remain well confined in the core, while the low energy ones leave the plasma at a rate that is high enough to avoid fuel dilution. This shows the importance of studying the energy dependence of the alpha particle redistribution produced by internal kink modes and how it varies with the mode and plasma parameters.

The redistribution of high energy ions by sawteeth has been extensively studied, both experimentally and theoretically. Experiments have shown that fusion born alpha particles and high energy ions resulting from neutral beam injection or wave heating can be substantially redistributed by internal kink modes with low toroidal (n) and poloidal (m) mode numbers.[1–4] In addition, experiments at JET have shown that sawteeth prevent the accumulation of impurities at the plasma center.[5] Since most experiments can only measure alpha particles in a relatively narrow energy range, there is little information about the energy dependence of particle redistribution. The experimental information about the spatial structure and temporal dependence of the modes that produce the redistribution is also limited.

Theoretical studies of alpha particle redistribution due to sawteeth can be broadly classified in two groups. One group includes those studies that assume full reconnection and employ a phenomenological description of the evolution of the flux surfaces, generally, including only the dominant (1, 1) kink mode. The other group includes the studies that directly employ the information about the spatial and temporal evolution of the modes present in a sawtooth to calculate the trajectories of the alpha particles. The approach employed in the studies included in the first group[6–8] appears to be better suited for sawteeth that exhibit full reconnection while the one used in those included in the second group[9–11] provides a more accurate description of the dynamics of alpha particles in sawteeth with partial reconnection and can include the effect of field line stochasticity.

In this paper, we present a detailed and systematic study of the energy and frequency dependence of the alpha particle redistribution produced by the internal kink modes associated with sawteeth with partial reconnection. The method employed in this study was introduced and discussed in detail in Refs. 10 and 11. In Ref. 11, we considered alpha particles with energies above 0.5 MeV and modes with a fixed frequency. Here, we extend those results by considering particles with energies down to 18 keV and modes with different frequencies. The results show that at lower energies, the redistribution of alpha particles is more sensitive to the mode frequency and particle energy. There are maxima and minima of the particle redistribution parameter (see below) which

depend on the frequency and number of modes present and on the particle energy. In particular, there are conditions where relatively high energy particles (i.e., $E \simeq 400$ keV) spread out much more than low energy particles ($E < 100$ keV).

The structure of this paper is as follows. In Sec. II, we briefly review the method presented in Refs. 10 and 11 to calculate the fields, and in Sec. III, the method employed to determine the initial conditions and the calculation of the trajectories of the particles. Section IV contains the results of the numerical calculations. Finally, in Sec. V, we summarize our findings and present the conclusions.

II. EQUILIBRIUM AND PERTURBED FIELDS

Here, we briefly review the method employed in Refs. 10 and 11 to calculate the equilibrium and perturbed fields. A complete justification of the assumptions and approximations employed can be found in those references. The equilibrium magnetic field is obtained from an analytic solution of the Grad-Shafranov equation for a toroidal plasma with circular cross section. Assuming that the pressure and poloidal current depend on the poloidal flux as $p = p_1\psi^2$; $I^2 = I_0^2 + I_1^2\psi^2$, where ψ is the poloidal flux and p_1, I_0^2 and I_1^2 are constants, we obtain (Gaussian units are used)

$$\psi(x,\theta) = C\left\{J_0(kx) + \frac{\cos\theta}{2}\left[xJ_0(kx) + \frac{\sigma J_1(kx)}{k}(1-x^2)\right]\right\}, \tag{1}$$

where x is the normalized minor radius ($x = \rho/a$, a: minor radius), θ the poloidal angle, and $J_0(kx)$ and $J_1(kx)$ are Bessel functions. The poloidal flux is normalized with $B_0\pi a^2$, where B_0 is the external toroidal field at the geometric axis (R_0), p is normalized with $B_0^2/8\pi$ and I with $B_0cR_0/2$. The other quantities appearing in Eq. (1) are $\sigma = 4p_1/\varepsilon^2$ and $k^2 = 4(p_1 + I_1^2)/\varepsilon^2$, where ε is the inverse aspect ratio. The boundary of the plasma is at the $x = 1$ surface, where $\psi = 0$. The constant C is determined by fixing the poloidal field at the plasma boundary (total toroidal plasma current) and I_0 is related to the vacuum toroidal field. Since we normalize all the fields with the vacuum toroidal field at R_0, $I_0 = 1$. Finally, σ, which is proportional to p_1, fixes the plasma β. Figure 2 of Ref. 10 shows the q profile and flux surfaces obtained with $\varepsilon = 1/3$, $p_1 = 0.05$, $B_{pol}(x = 1, \theta = 0) = 0.155$ (note that $q_0 = 0.83$).

Ideal MHD is used to calculate the perturbed electric and magnetic fields

$$\mathbf{B}_1 = \nabla \times (\xi \times \mathbf{B}), \quad \mathbf{E}_1 = -\frac{v_1 \times \mathbf{B}}{c}, \quad v_1 = \frac{\partial \xi}{\partial t}, \tag{2}$$

where $\mathbf{E}_1$ and $\mathbf{B}_1$ are the normalized (with B_0) perturbed electric and magnetic fields, ξ is the displacement, normalized with the minor radius (a), and $\mathbf{B}$ the normalized equilibrium magnetic field.

The sawtooth cycle is characterized by a slow rise of the central temperature and density, followed by a fast reduction (crash). The amplitude of the (1, 1) internal kink mode shows a similar behavior, with a post crash value that depends on the amount of reconnected flux. The other modes considered here, (2, 2) and (2, 1), are driven by the (1, 1) mode and begin to grow when the amplitude of the (1, 1) mode is large enough. We employ here the same time dependence used in Ref. 11, which matches the experimental results presented in Ref. 12. This corresponds to a case with partial reconnection, where the (1, 1) mode does not disappear after the crash and the safety factor remains below one at the magnetic axis. The spatial dependence is also the same as in Ref. 11, except that the values of x_s and x_{22} were reduced slightly ($x_s = 0.4$, $x_{22} = 0$) to obtain smaller amplitudes for the (1, 1) and (2, 2) modes at the $q = 1$ surface. The x component of the displacement is therefore written as

$$\begin{aligned}\xi_x(x,\phi,\theta,t) = {} & \xi^{11}(t)f_{11}(x)\cos(\theta - \phi - \omega_{11}t) \\ & + \xi^{22}(t)f_{22}(x)\cos[2(\theta - \phi - \omega_{11}t)] \\ & + \xi^{21}(t)f_{21}(x)\cos(2\theta - \phi - \omega_{21}t),\end{aligned} \tag{3}$$

where ω_{11} and ω_{21} are the frequency of oscillation of the (1, 1) and (2, 1) modes and $\xi^{mn}(t)$ and $f_{mn}(x)$ are chosen to match the space and time dependence observed in the experiments. The ratio ω_{21}/ω_{11} is fixed at 2.65, value reported in Ref. 9.

III. INITIAL CONDITIONS AND NUMERICAL METHODS

The exact trajectories of a large number of alpha particles were followed to determine the redistribution produced by the modes considered. The methods used to determine the initial conditions (position and velocity) of the alpha particles and integrate their trajectories are the same ones employed in Ref. 11. A slowing down distribution function was used to determine the initial density profiles of particles with a given energy. The distribution function employed is probably not very accurate at low energies but was used to allow a simple, continuous energy variation from 3.5 MeV down to 18 keV.

Our simulations start when the amplitude of the (1, 1) mode is 70% of its maximum value and the other modes begin to grow. We have shown in Ref. 11 (see Fig. 3) that changing the starting time and the temporal evolution of the amplitude of the (1, 1) mode does not produce significant changes in the final results. Collisions are not included. Since the simulation time is approximately 1.5 ms, this approximation is well justified for energies above 100 keV but begins to fail at lower energies.

In the equations of motion, the time is normalized with Ω_α (cyclotron frequency calculated with the vacuum toroidal field at R_0), lengths are normalized with the minor radius (a), and velocities with the initial velocity of the alpha particle (v_0). This results in a single dimensionless parameter appearing in the normalized equations

$$\gamma = \frac{v_0}{\Omega_\alpha a}.$$

With ITER like parameters ($B_0 = 5.3$ T, $a = 2$ m), $\gamma = 2.552 \times 10^{-2}$ for a 3.5 MeV alpha particle and decreases as the square root of the energy for lower energies. We note that a 40 keV deuteron in the DIII-D discharge employed in Ref. 4 has a γ of approximately 3.5×10^{-2}; an alpha particle in ITER would need an energy of approximately 6.6 MeV to have the same value of γ.

Particles can be divided in trapped, co-passing (rotate in the same sense as the plasma current), and counter-passing (rotate in the opposite sense). To quantify the spreading of

each type of particle, we first introduce a parameter that measures the width of the distribution of that type at a given time

$$\sigma_s^2(t) = \frac{1}{N_s}\sum_{i=1}^{N_s}\left\{[r_i(t) - \bar{r}_s(t)]^2 + [z_i(t) - \bar{z}_s(t)]^2\right\},$$

where s indicates the type of particle and N_s the total number of particles of that type. The averages $\bar{r}_s(t)$ and $\bar{z}_s(t)$ are calculated considering all the particles of a given type. Note that particles can change their status and this will change the value of N_s and the specific particles included in the calculation. Having $\sigma_s^2(t)$, we can define a parameter that measures the spreading of each type of particle as a function of time

$$\chi_s(t) = \frac{\sigma_s^2(t)}{\sigma_s^2(t=0)}.$$

We also introduce a parameter that measures the total spreading of the particles

$$\chi(t) = \frac{\sigma^2(t)}{\sigma^2(t=0)}.$$

In this case, $\sigma^2(t)$ is calculated using all the particles

$$\sigma^2(t) = \frac{1}{N}\sum_{i=1}^{N}\left\{[r_i(t) - \bar{r}(t)]^2 + [z_i(t) - \bar{z}(t)]^2\right\},$$

where N is the total number of particles and $\bar{r}(t)$ and $\bar{z}(t)$ are calculated using all the particles. Note that due to the differences between $\bar{r}(t)$ and $\bar{r}_s(t)$, the total $\sigma^2(t)$ is not the weighted sum (with the fraction of each type of particle) of the $\sigma_s^2(t)$. The parameters defined above are somewhat different from those used in Ref. 11. The assumptions regarding the density and temperature profiles are the same as those used in Ref. 11.

IV. RESULTS

A. (1, 1) and (2, 2) modes

First, we calculate the particle redistribution produced when only the (1, 1) mode is present. Figure 1 shows a plot of the total χ_f (final value of χ considering all the particles) as a function of the energy for $\xi_0^{11} = 0.12$ and four different frequencies. We note that for $E > 1000$ keV, χ_f increases slowly with the energy (probably due to the larger orbit size) and also with the frequency (probably due to the increasing electric field). On the other hand, for $E < 1000$ keV, there is a strong energy and frequency dependence. Depending on the mode frequency, lower energy particles can be more or less redistributed than higher energy ones. In addition, for $\omega_{11} = 2 \times 10^{-4}$ and 4×10^{-4}, there is a minimum in χ_f at an energy that increases with the mode frequency. For $\omega_{11} = 1$ and 0.5×10^{-4}, the minimum is probably at a lower energy than the minimum value shown in these plots (18 keV). Although not shown in the plots, because for very low energies, some of the approximations employed in this study (slowing down distribution function, collisionless) are not valid, we continued our calculations down to $E = 1$ keV. The results show that for $\omega_{11} = 4 \times 10^{-4}$, there is a maximum of χ_f at $E \simeq 8$ keV and for $\omega_{11} = 2 \times 10^{-4}$ at $E \simeq 2$ keV.

Since the effect of the perturbation depends on the type of particle (trapped, co-passing or counter-passing), it is necessary to consider each type separately to understand the results presented in Fig. 1. Figure 2 shows a plot of χ_f as a function of the energy for $\xi_0^{11} = 0.12$ and $\omega_{11} = 2 \times 10^{-4}$. In this plot, three curves are labeled according to the type of particle, while the fourth one shows the value of the total χ_f (as in Fig. 1). The first feature to note is that different types of particles behave differently. Another important aspect is that high energy particles can be redistributed as much as low energy ones. The χ_f of counter-passing particles is approximately constant between 500 keV and 2 MeV and decreases slowly at higher energies. Below 500 keV, χ_f decreases, reaches a minimum at approximately 75 keV and increases rapidly at lower energies. Note that the values at 18 keV and 1000 keV are basically the same. The χ_f of co-passing particles is small, and almost constant, with a small increase at low energy. Trapped particles have a broad minimum around 600 keV, a small relative maximum at 250 keV, and a rapid increase below 100 keV. Above 1 MeV, the χ_f of trapped particles increases almost linearly with the energy.

As indicated above, we continued our calculations down to $E = 1$ keV to try to explain the rapid increase in χ_f at low

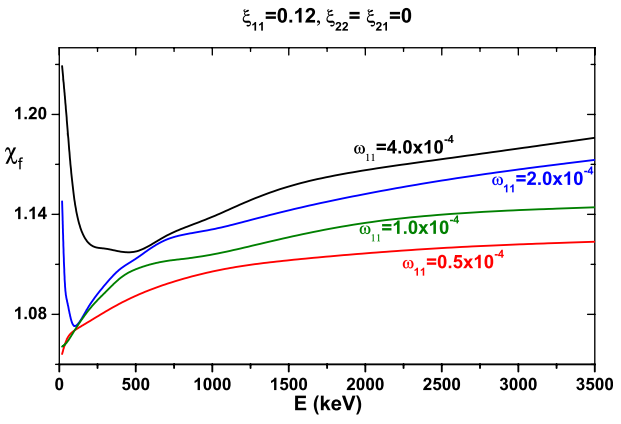

FIG. 1. Final value of the total χ as a function of the energy for $\xi_0^{11} = 0.12$ and four different frequencies.

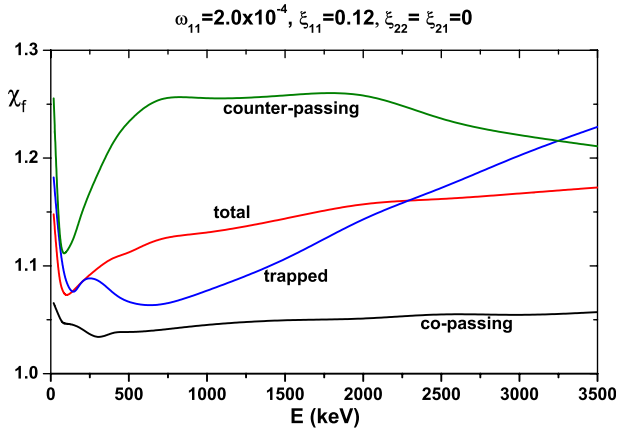

FIG. 2. χ_f vs. energy for each type of particle (co-passing, counter-passing, and trapped) and the total.

energies. For $\omega = 2 \times 10^{-4}$ (value used in Fig. 2), the χ_f of counter-passing particles has a maximum around 2–3 keV, while for $\omega = 4 \times 10^{-4}$, the maximum is at 8–10 keV. The factor four increase in energy for a factor two increase in mode frequency indicates that the low energy peaks could be due to a resonance between the mode and the periodic rotation of the particles (the period of particle rotation decreases as $\sqrt{E}$). It should be noted, however, that the alpha particles have random pitch and are distributed on different flux surfaces. This indicates that there will be a distribution of periods for each type of particle and therefore no sharp resonances. At low energy and with relatively small perturbations, the guiding center approximation should be valid. In the large aspect ratio limit (valid inside the $q = 1$ surface), a mode with toroidal and poloidal numbers n and m resonates with a passing particle when the following condition is satisfied:[13]

$$\left[n - \frac{m \pm 1}{q}\right]\omega_t = \omega_{mn},$$

where ω_t is the toroidal transit frequency of the passing particle. In our case, with $n = m = 1$, a resonance with a counter-passing particle occurs when

$$\left[1 - \frac{2}{q}\right]\omega_t = \omega_{mn} \Rightarrow \omega_t = \frac{\omega_{mn}}{\frac{2}{q} - 1}.$$

In our equilibrium, the minimum value of q is 0.83 and the mode extends to the $q = 1$ surface. Taking $q = 0.9$, we obtain $\omega_t = 1.636 \times 10^{-4}$ which is similar to the average transit frequency obtained for $E = 2$ keV. We therefore conclude that the rapid increase in the χ_f of counter-passing particles at low energies is due to a mode particle resonance which produces a peak at very low energies. Above 500 keV, χ_f changes slowly and particle redistribution cannot be correlated with specific resonances. The χ_f of trapped particles has a maximum at approximately 8 keV, where the bounce frequency is approximately half the mode frequency.

Additional insight into the mechanisms involved in particle redistribution can be obtained by analyzing what occurs with the constant of motion and the adiabatic invariants. This is shown in Appendix.

Figures 3(a)–3(f) show the initial and final density profiles of the three types of particles for $E = 50$ and 400 keV, $\xi_0^{11} = 0.12$, and three different frequencies. It can be seen that consistent with the values of χ_f presented in Fig. 2, trapped and counter-passing particles can be significantly redistributed while co-passing particles are only weakly redistributed. In general, but not always, the redistribution increases with the mode frequency. For example, the peak density of 50 keV trapped particles decreases to approximately 96%, 83%, and 65% of the initial value for $\omega_{11} = 0.5$, 2, and 4×10^{-4}, respectively. The redistribution occurs mostly inside the $q = 1$ surface and the particles do not reach the plasma boundary. The peak density of counter-passing particles decreases to between 67% and 84% of its initial value, depending on the mode frequency and particle energy. For $\omega_{11} = 4 \times 10^{-4}$ (curve 2 in Fig. 3(c)), the final density profile of 50 keV counter-passing particles presents two "shoulders" next to the $q = 1$ surface. This is due to the particles being pushed against the $q = 1$, where the sharp drop in the mode amplitude prevents further displacements.

The effect produced in the particle redistribution by changes in the mode amplitude depends on the frequency. This is shown in Figure 4, which is similar to Figure 1 but has $\xi_0^{11} = 0.30$. For $\omega_{11} = 0.5$ and 2×10^{-4}, the qualitative behavior is the same but with a larger particle redistribution. For $\omega_{11} = 4 \times 10^{-4}$, the response changes significantly because the minimum observed for $\xi_0^{11} = 0.12$ disappears

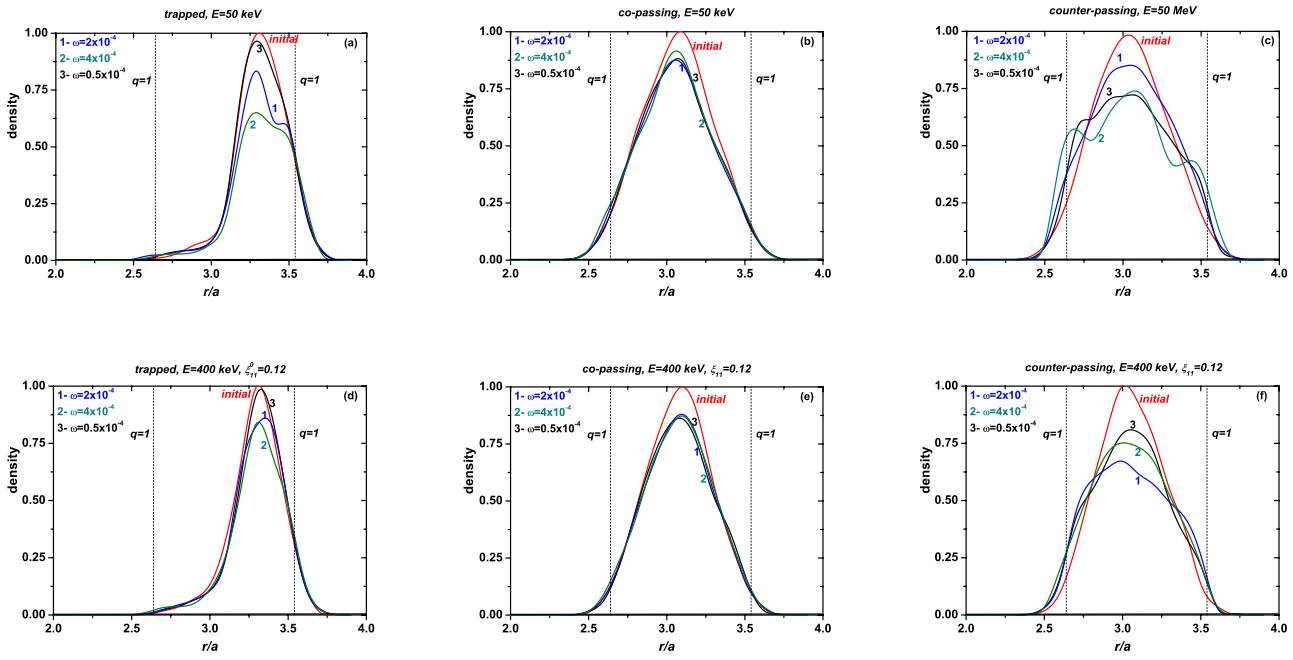

FIG. 3. Initial and final density profiles of the three types of particles for E = 50 and 400 keV, $\xi_0^{11} = 0.12$, and three different frequencies.

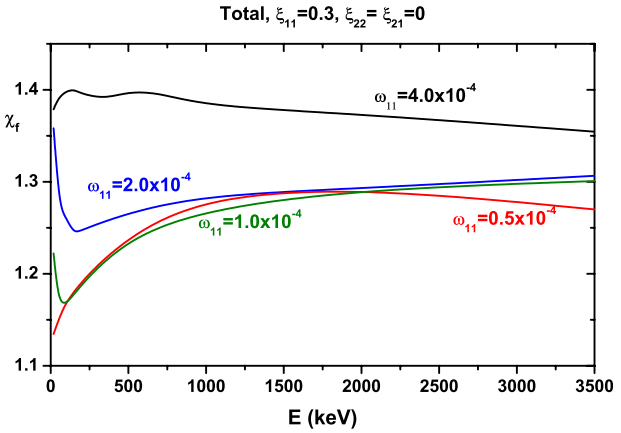

FIG. 4. Total χ as a function of the energy for $\xi_0^{11} = 0.3$ and different mode frequencies.

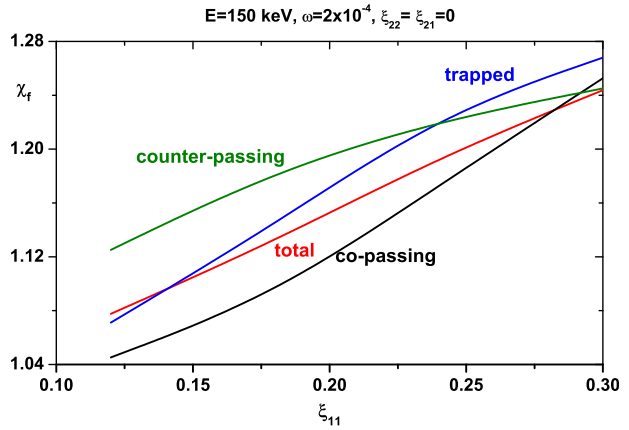

FIG. 6. χ as a function of the (1, 1) mode amplitude for $E = 150$ keV and $\omega = 2 \times 10^{-4}$.

and χ_f remains almost constant over the entire energy range. For $\omega_{11} = 1 \times 10^{-4}$, the behavior at high energy is qualitatively the same but a minimum, followed by a rapid increase appears at low energy.

Figures 5(a) and 5(b) present additional information on the effect of changing the mode amplitude. This figure has plots of the total density profiles for $\xi_0^{11} = 0.30$, $E = 50$, and 400 keV and various frequencies. We can see that for this mode amplitude, the peak value can be reduced as much as 50% and that higher frequency modes generally produce a larger reduction. The change in the profiles appears to be larger in the higher field side but it should be weighted by the radius reduction. Figure 6 is a plot of χ_f as a function of the mode amplitude for $\omega = 2 \times 10^{-4}$, $E = 150$ keV, and different types of particles. It can be seen that the total χ_f increases almost linearly with the mode amplitude but the rate of increase is different for different types of particles.

We mentioned above that the interaction with the modes can change the status of the particles. This is seen in Figure 7, where we show the fraction of particles whose final status is different from the initial as a function of the energy for different frequencies and mode amplitudes. This does not include those particles that change between two statuses an even number of times. It is clear that this fraction can be large, depending on the frequency and mode amplitude. Except for the reduction at very low energies shown for $\xi_0^{11} = 0.30$ and $\omega_{11} = 4 \times 10^{-4}$, the fraction decreases with the energy and mode frequency.

To conclude this section, we show in Figures 8(a) and 8(b) the effect of adding a (2, 2) mode. Figure 8(a) shows the total density profile for $E = 150$ keV, $\xi_0^{11} = 0.30$, $\omega = 2 \times 10^{-4}$, and different values of ξ_0^{22}, and Figure 8(b) shows the change in χ_f for the same parameters. Although relatively large changes occur when the amplitudes of the (2, 2) and (1, 1) mode are equal we should note that for the same displacement amplitude, the perturbed fields associated with the (2, 2) mode would be significantly larger than those associated with the (1, 1) mode. When $\xi_0^{22}/\xi_0^{11} = 1/3$, ratio employed in most of our studies, the addition of the (2, 2) mode produces only minor changes.

B. Effect of the (2, 1) mode

The addition of a (2, 1) mode increases particle spreading and changes the response of the different types of particles. As noted in Ref. 11, regions of stochasticity appear when a mode with different helicity is added. Figure 9 shows a plot of the total χ_f as a function of the energy for $\xi_0^{11} = 0.12$, $\xi_0^{21} = \xi_0^{22} = 0.04$, and four different frequencies. The curves corresponding to $\omega_{11} = 4 \times 10^{-4}$, 2×10^{-4}, and 1×10^{-4} ($\omega_{21} = 2.65\ \omega_{11}$) have maxima at $E \simeq 1250$ keV, $E \simeq 300$ keV, and $E \simeq 75$ keV, respectively. We note that the energy corresponding to the maximum changes by a factor approximately equal to 4 when the frequency changes by a factor 2, indicating the possibility of a resonance with a periodic particle motion having a frequency proportional to $\sqrt{E}$. The curve corresponding to $\omega_{11} = 0.5 \times 10^{-4}$ has a smooth maximum at high energy ($E \simeq 3000$ keV) and a sharp increase at low energies but without reaching a maximum, which should be located around 18 keV.

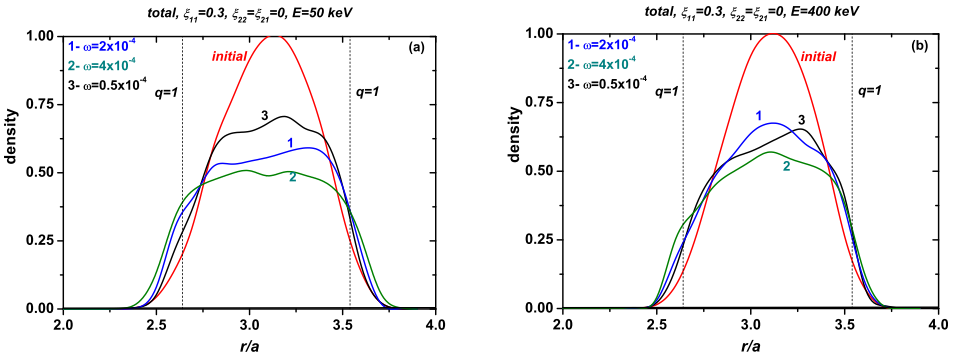

FIG. 5. Total density profiles for $\xi_0^{11} = 0.3, E = 50$ and 400 keV and different mode frequencies.

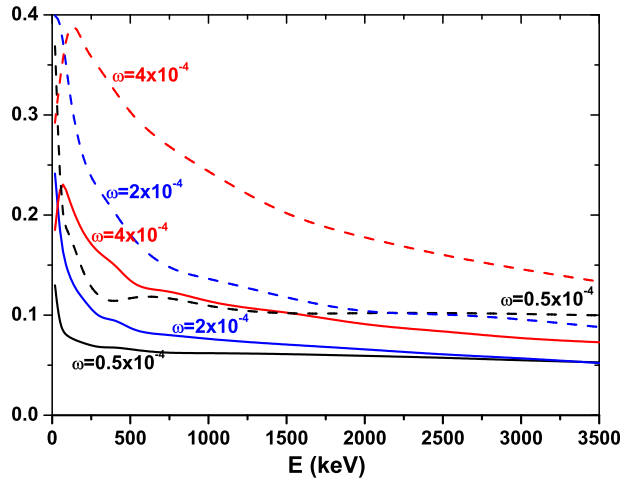

FIG. 7. Fraction of particles that change their status for different frequencies and mode amplitudes. The curves are labeled according to the mode frequency and the mode amplitude is 0.12 for full line curves and 0.3 for dashed curves.

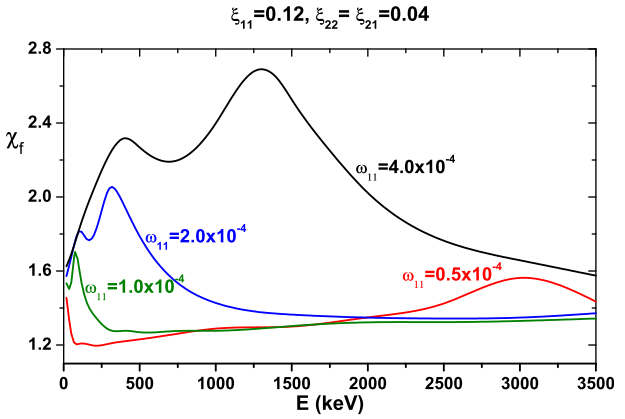

FIG. 9. Total χ_f as a function of the energy for different frequencies. The (1, 1), (2, 2), and (2, 1) modes are included.

Figure 10 shows a plot of the χ_f corresponding to different types of particles as a function of the energy (as in Fig. 2) for the same mode amplitudes as in Figure 9 and $\omega_{11} = 2 \times 10^{-4}$. It can be seen that the χ_f of trapped particles has a large peak at the same energy as the peak shown in Fig. 9 for this frequency. Although not shown here, the same behavior is observed for the other mode frequencies. We therefore conclude that the maxima seen in the total χ_f (Fig. 9) are due to trapped particles that experience a large redistribution. To elucidate the mechanism responsible for the redistribution of trapped particles, we constructed plots of the distribution of periods for the periodic motion of the different types of particles. The periodic particle motions have a distribution of periods similar to that shown in Figures 5 and 6 of Ref. 10. For $E = 1250$ keV, the bounce frequency of trapped particles is approximately the same as the frequency of the (2, 1) mode in the $\omega_{11} = 4 \times 10^{-4}$ curve ($\omega_{21} = 10.6 \times 10^{-4}$) and the precession frequency is much smaller. This indicates that the maximum could be due to a resonance between the bounce motion of trapped particles and the (2, 1) mode. Since the bounce frequency is proportional to $\sqrt{E}$, the same argument applies to the maxima observed in the other curves. It is not clear, however, why the combined effect of three modes with different frequencies produces a resonance with only one of the modes (unless the amplitude of the perturbed fields associated with the (2, 1) mode is much larger than the others). This is further complicated by the fact that a much smaller maximum appears if only the (2, 1) mode is included. We therefore need a mechanism that requires the presence of the (1, 1) and (2, 2) modes but produces a resonance at the frequency of the (2, 1) mode. A possible explanation is that when all the modes are present, the magnetic field becomes stochastic and a large particle redistribution occurs. Particles move outwards, increasing the fraction of trapped particles, and a large fraction of the particles reaches a minor radius where the (1, 1) mode has already vanish and therefore are only affected by the (2, 1) mode.

To support the explanation provided above, we show in Figure 11 a plot of the χ of different types of particles as a function of time for $\omega_{11} = 2 \times 10^{-4}$, $\xi_0^{11} = 0.12$, $\xi_0^{21} = \xi_0^{22} = 0.04$, and $E = 400$ keV. This plot shows that initially counter-passing particles spread out faster than trapped particles but later, the χ of trapped particles increases faster, and is significantly larger than the others at the crash. Another interesting feature of this plot is that the crash does not produce significant changes in the values of χ. This was already reported in Ref. 11 and is due to the stochasticity of the magnetic field. In Figure 9, the curves with $\omega_{11} = 4 \times 10^{-4}$ and 2×10^{-4} have a second, smaller, maximum at $E \simeq 400$ keV and $E \simeq 100$ keV, respectively. The energy ratio is 4 again, for a frequency ratio of 2. The energy ratio between the two maxima of the same curve is approximately 3. These maxima are also due to the trapped particles, as can be seen by looking at the χ_f of trapped particles in Figure 10.

Figures 12(a)–12(f) show the initial and final density profiles of the three types of particles for $E = 50$ and

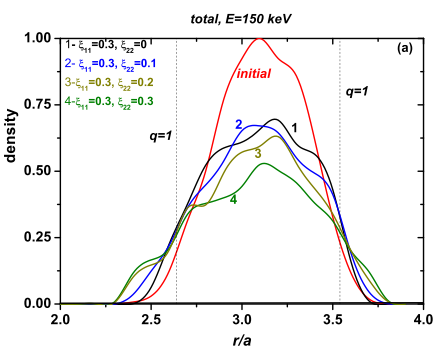

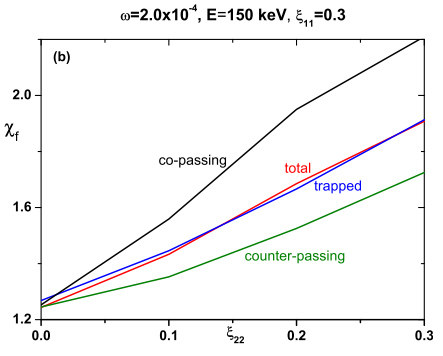

FIG. 8. Effect of increasing the amplitude of the (2,2) mode for $E = 150$ keV and $\omega = 2 \times 10^{-4}$.

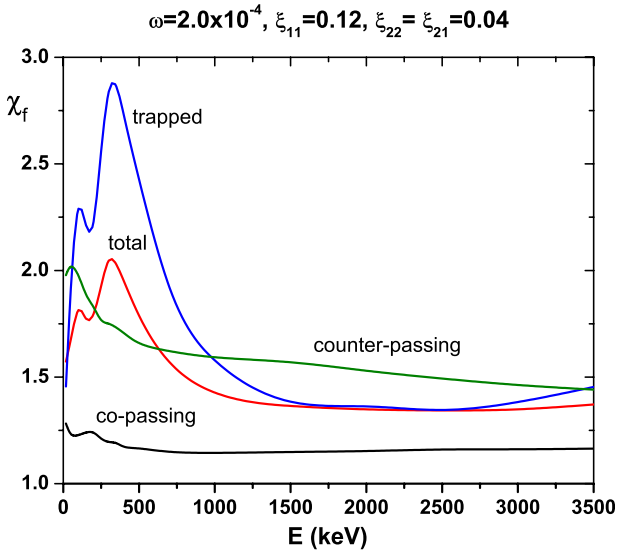

FIG. 10. χ_f vs. energy for each type of particle (co-passing, counter-passing, and trapped) and the total.

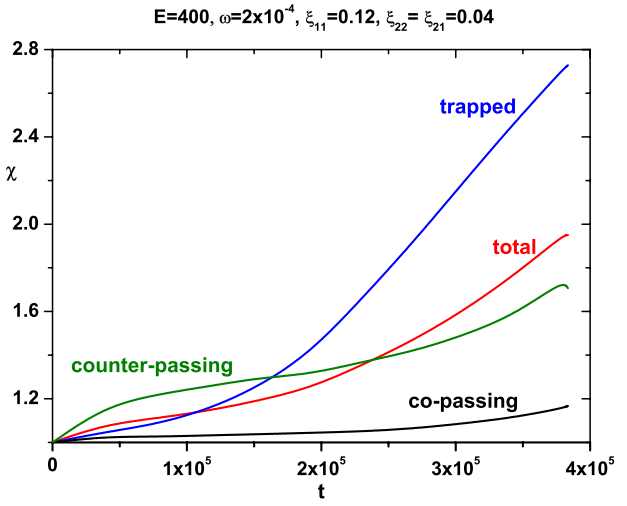

FIG. 11. χ as a function of time for different types of particles. Time is normalized with the cyclotron frequency at the geometric axis.

400 keV, $\xi_0^{11} = 0.12$, $\xi_0^{21} = \xi_0^{22} = 0.04$, and three different frequencies. We see that trapped and counter-passing particles are strongly redistributed while co-passing particles are less affected. The peak densities of trapped and counter-passing particles can be reduced to approximately half and one third of their initial values, respectively. Since the (2, 1) mode extends beyond the $q = 1$ surface, particles can reach the edge of the plasma.

The effect of increasing the mode amplitude is shown in Figure 13, which presents a plot of χ_f as a function of the energy for $\xi_0^{11} = 0.3$, $\xi_0^{21} = \xi_0^{22} = 0.1$, and three different frequencies. Comparing with Figure 9, we see that the basic features are similar but the values of χ_f are almost double. In the curves with $\omega_{11} = 4$ and 2×10^{-4}, the secondary peaks almost disappear and so does the high energy maximum in the $\omega_{11} = 0.5 \times 10^{-4}$ curve. Additional information on the effect of increasing the mode amplitude is presented in Figures 14(a) and 14(b), which shows the total density profiles for the same mode amplitudes, $E = 50$ and 400 keV and three mode frequencies. It can be seen that the peak density can be reduced to less than 25% of its initial value and a minimum can appear at the magnetic axis in some cases. Alpha particles can reach the edge of the plasma and a small fraction is actually lost in this case. The maximum loss occurs for $E \simeq 1500$ keV (around the maximum of χ_f) and is approximately 1.5% of the total.

The effect of changing the amplitude of the modes, keeping constant the ratio $\xi_0^{11}/\xi_0^{22} = \xi_0^{11}/\xi_0^{21} = 3$, is shown in Figure 15, which presents a plot of the χ_f of different types of particles as a function of the mode amplitude for $E = 150$ keV, $\omega_{11} = 2 \times 10^{-4}$. We note again that although

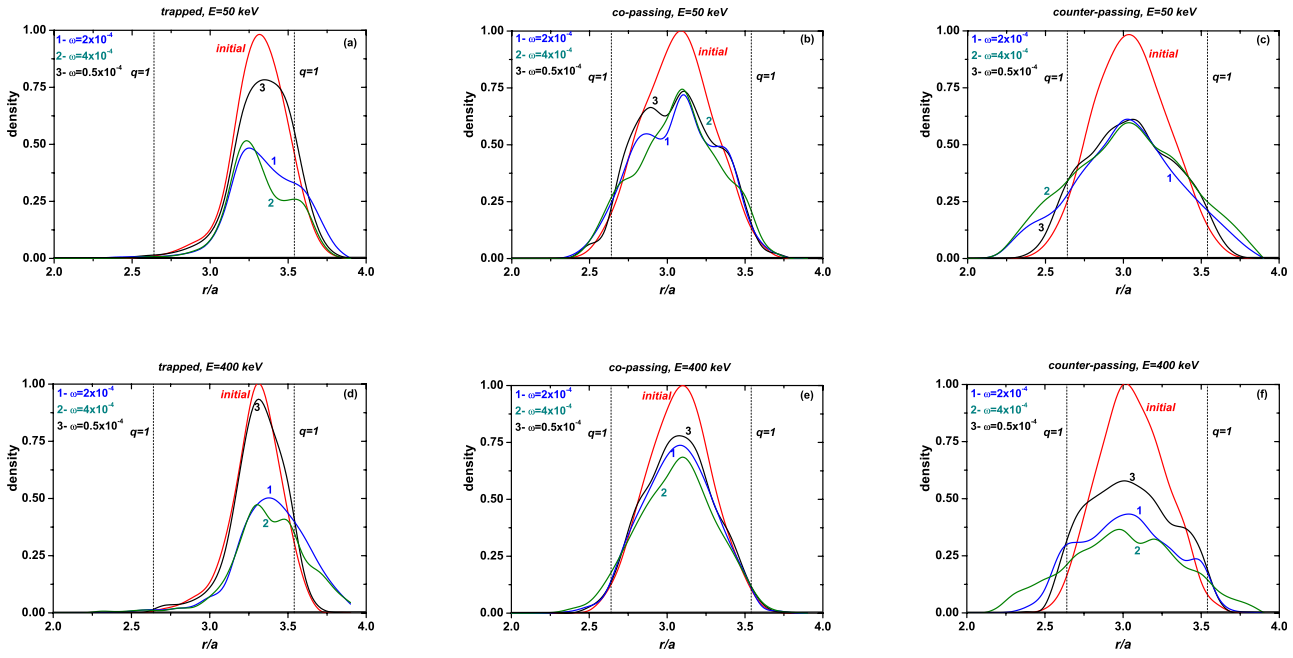

FIG. 12. Initial and final density profiles of the three types of particles for E = 50 and 400 keV, $\xi_0^{11} = 0.12$, $\xi_0^{22} = \xi_0^{21} = 0.04$, and three different frequencies.

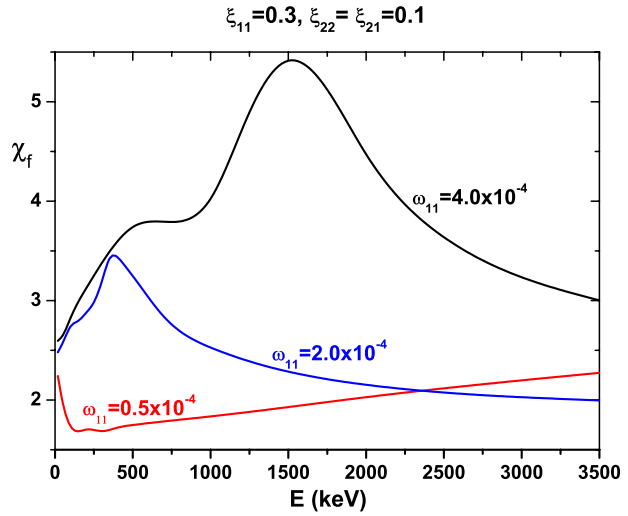

FIG. 13. Total χ_f as a function of the energy for different frequencies. The (1, 1), (2, 2), and (2, 1) modes are included with $\xi_0^{11} = 0.3$, $\xi_0^{22} = \xi_0^{21} = 0.1$.

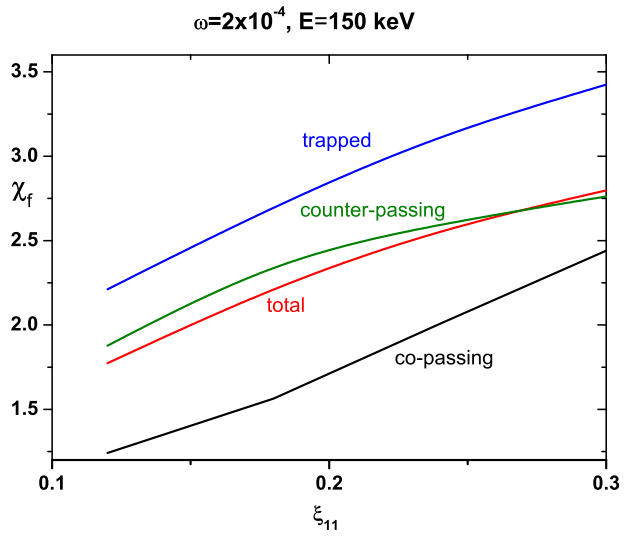

FIG. 15. χ_f as a function of the amplitude of the modes with $\xi_0^{11}/\xi_0^{22} = \xi_0^{11}/\xi_0^{21} = 3$.

the spreading of all the particles increases with the mode amplitude, the rate at which they do it is different.

To conclude this section, we show in Figure 16, the fraction of particles that change their status when all the modes are present as a function of the energy, for different amplitudes and frequencies (as in Figure 7). We note that, unlike the behavior shown by χ_f (see Figure 9), there are no maxima and, except for one case, the fraction of particles that change their status decreases with the energy.

V. SUMMARY AND DISCUSSION

We studied the effect of internal kink modes on the redistribution of alpha particles in plasmas with aspect ratio, toroidal field, and current density similar to those expected in ITER. All the relevant energy range (18 keV $\leq E \leq$ 3.5 MeV) and various mode frequencies and amplitudes were considered. This is an important topic because high energy particles are needed to heat the plasma but low energy ones should be removed to avoid diluting the fuel. In addition, the redistribution of alpha particles could affect the stability of the plasma. Our results show that the energy range of the particles that are most affected (larger redistribution) depends on the number, amplitude, and frequency of the modes present.

This work is the first one to present clear and conclusive evidence of the importance of the mode frequency on particle redistribution. None of the previous studies showed this. Zhao and White,[9] who used a similar approach, considered only one frequency value. The studies presented in Refs. 6–8 completely neglect the mode frequency and the effect of the precursor and postcursor modes. As a result, they conclude that the most important contribution to particle redistribution comes from the $\mathbf{E} \times \mathbf{B}$ drift, where the electric field is associated with the temporal evolution of the helical perturbation at the crash. We show that for our conditions, the most important contribution comes from the electric field produced by the rotation of the mode.

This, and our previous studies,[10,11] are the only ones where the perturbed fields are calculated directly, using ideal MHD, without the assumptions introduced in Ref. 9. In addition, our studies are the only ones where the exact particle orbits have been used. We show that the addition of modes with different helicities (from that of the (1,1)), which can lead to the stochastization of the magnetic field, can greatly increase particle redistribution. This is already indicated in Ref. 9, but we present a more detailed study, where the relative amplitudes of the mode are changed, and different mode frequencies are considered.

The use of a simple analytical equilibrium with circular cross section allows us to obtain analytical expressions for the perturbed fields, thus simplifying the numerical calculations and reducing the required computational time. ITER plasmas will have a "D" shaped cross section with

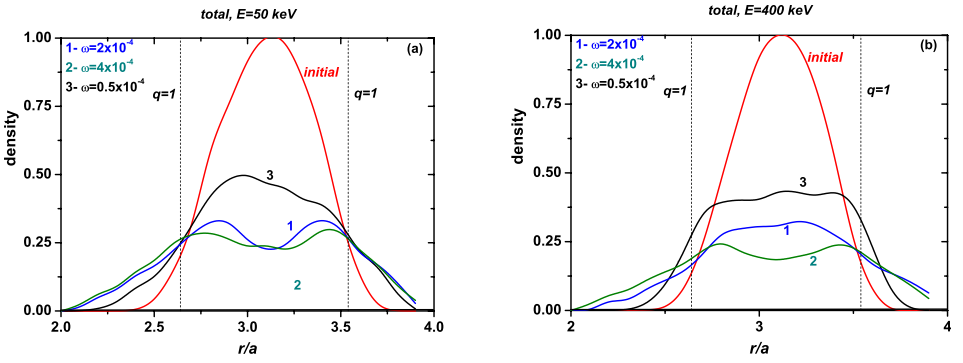

FIG. 14. Total density profiles for $\xi_0^{11} = 0.3$, $\xi_0^{22} = \xi_0^{22} = 0.1$, $E = 50$, 400 keV, and different mode frequencies.

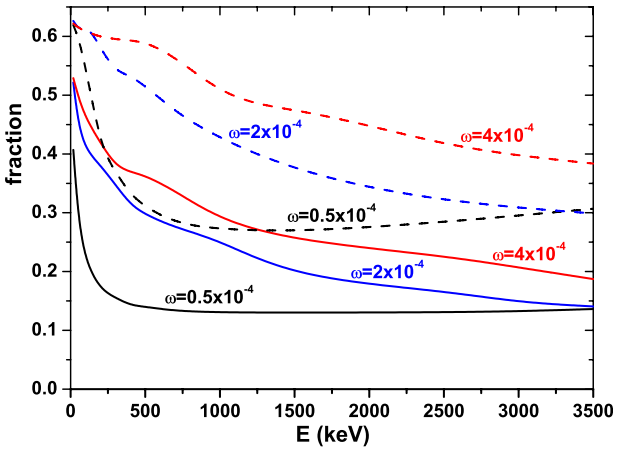

FIG. 16. Fraction of particles that change their status for different frequencies and mode amplitudes. The curves are labeled according to the mode frequency and the mode amplitude is 0.12 for full line curves and 0.3 for dashed curves.

elongation (κ) and triangularity (δ) at the 95% flux surface equal to 1.70 and 0.33, respectively, but the values of these parameters at the inner flux surfaces, in particular, inside the $q=1$ surface, will be significantly smaller. Using an ITER like cross section should therefore produce only small changes in the values of the energy and frequency corresponding to maxima and minima of the redistribution parameter (χ), without changing the basic features of the results presented here.

The main results can be summarized as follows:

1. When only the (1, 1) mode is included, the spreading of high energy (E > 1 MeV) alpha particles increases slowly with the energy and mode frequency. At lower energies, the redistribution is more sensitive to the mode frequency and particle energy. Depending on the mode frequency, lower energy particles can be more or less redistributed than higher energy ones.
2. When a single mode is present, the most important contribution to particle redistribution comes from the electric field produced by the rotation of the mode. For our conditions the electric field produced at the crash makes a very small contribution. Increasing the duration of the crash by a factor four, from the 15 μs normally used in the simulations to 60μs, changes the value of χ by less than 1%.
3. The addition of a (2, 1) mode, which can produce the stochastization of the magnetic field, significantly increases particle redistribution. Particles can spread beyond the q = 1 surface and leave the plasma. Its effect depends on the energy of the particles and the amplitude of the other modes.
4. When only the (1, 1) mode is included, counter-passing particles, which rotate in the sense of mode propagation, are the most affected. When the (2, 1) mode is included, trapped particles are the most affected.
5. The fraction of particles that change their status can be significant, depending on the energy and number and amplitude of the modes present.

Our results show that the kink modes associated with sawtooth oscillations could have a larger effect on relatively high energy particles than in what can be considered helium ash. Since the redistribution depends on the frequency and amplitude of the modes, it should be possible to control particle redistribution by acting on these parameters. The mode amplitude is related to the sawtooth period, which can be controlled by external heating.[14] The mode frequency is due to diamagnetic effects and plasma rotation,[15] which can be controlled with neutral beam injection.

For obvious reasons, the experimental information available on the effect of sawteeth on alpha particles is limited. Additional experiments are needed to obtain the information required to test the existing models and simulations. It is very important to perform these experiments with particles having the same value of γ as alpha particles in ITER and to obtain detailed information on the mode number, amplitude, and frequency of the perturbations.

ACKNOWLEDGMENTS

Financial support from the ECOS-MINCyT Research Grant No. A09E02 is gratefully acknowledged.

APPENDIX: PARTICLE ORBITS AND CONSTANTS OF MOTION

The analysis of particle orbits and the evolution of the constants of motion can provide some information about the mechanisms involved in particle redistribution. Here, we consider the simplest case, where only a relatively low amplitude (1, 1) mode is present. In the plots presented below, particle trajectories are constructed by calculating the instantaneous position of the guiding center from the exact orbit. In all cases, the particle is initially at $r=3.3$, $z=0$, $\phi=5.5$ and the initial pitches of trapped and counter passing particles are the same for both energies. The toroidal rotation periods of the counter passing particles are 1.18×10^4 and 0.16×10^4 and the bounce periods are 6.25×10^4 and 0.78×10^4, respectively, for the 18 keV and 1 MeV particles. The perturbation employed has $\xi_0^{11}=0.12$ and $\omega=2\times10^{-4}$.

In a static axisymmetric equilibrium, the energy and the toroidal component of the canonical momentum are exact constants of motion and the particles describe closed orbits. When a perturbation is introduced, these constants are destroyed and the particles can move across flux surfaces. Figure 17 shows the orbits of typical trapped and counter passing particles for three different situations: without perturbation, with perturbation, and with perturbation but with $\omega=0$. When $\omega=0$, the mode does not rotate but its amplitude changes. This means that there is a static magnetic perturbation and the only contribution to the perturbed electric field comes from the change in amplitude, which is significant at the crash.

We see in Fig. 17(a) that for $\omega=0$, the low energy counter passing particle remains circulating and its orbit covers a relatively small region around the initial flux surface. The final deviation of the particle, shown in red, is due to the electric field produced at the crash. When the full effect of the electric field is included ($\omega\neq0$), the width of the region

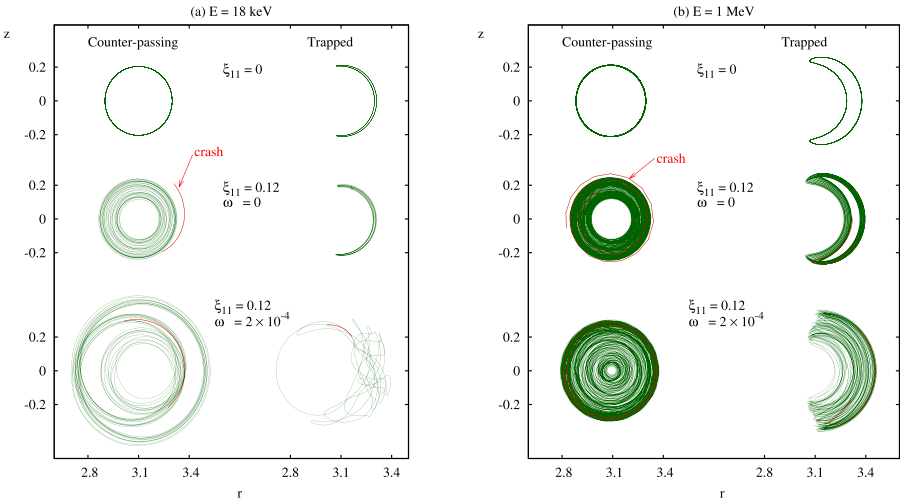

FIG. 17. Trajectories of typical counter passing and trapped particles. The trajectory after the crash is indicated in red.

visited by the particle increases significantly, the particle becomes barely trapped for some time and the crash does not have a large effect. The trapped particle executes a narrow banana orbit with turning points around $r = 3$. In the case $\omega = 0$, this particle remains trapped and suffers small displacements from its original orbit (not very clear in the figure). When $\omega \neq 0$, the particle changes to circulating for some time and a very complicated orbit results. It is clear that in this case, the radial displacement of the particle is much larger.

Figure 17(b) shows 1 MeV particles that have the same initial position and pitch as those shown in Fig. 17(a). The distance traveled by these particles and the width of the banana orbits are much larger than for the 18 keV particles. When $\omega = 0$, the orbit of the counter passing particle is similar to that of the 18 keV particle and the effect of the crash is barely noticeable. The orbit obtained when $\omega \neq 0$ is clearly different from that of the 18 keV particle. The 1 MeV particle remains circulating and visits a region with smaller minor radius. The trapped particle shows a similar behavior. When $\omega = 0$, the orbit moves slightly inwards and outwards without significant shape changes. When $\omega \neq 0$, the orbit displacements are larger but the particle remains trapped. We can summarize the results of Fig. 17 as follows:

1. When $\omega = 0$, the particles do not change their status and the perturbation has similar effect on the 18 keV and 1 MeV particles.
2. When $\omega \neq 0$, the 18 keV particles change their status but the 1 MeV ones do not.
3. The most important effect is produced by the electric field associated with mode rotation.

Figure 18 shows what happens with the constants of motion and the magnetic moment for the same conditions as in Fig. 17 (all quantities normalized to their initial values). Considering first the 18 keV counter passing particle, we note that when $\omega = 0$, the energy changes very slowly until the crash, where there is a 30% reduction. The P_ϕ shows a relatively low amplitude regular oscillation until the crash, where there is a small drop. The frequency of this oscillation is smaller than the transit frequency of the particle. The magnetic moment has a rapid, small amplitude, oscillation, and a small reduction at the crash. The changes produced at the crash can be correlated with the changes produced in the particle orbit, shown in red in Fig. 17(a). Since the energy is reduced, the particle moves to a larger minor radius.[13] When the full perturbation is added, the energy changes in a non periodic form, but the general pattern seems to repeat. The relative change can be more than 50% and the effect of the crash becomes negligible compared with the previous variations. The P_ϕ oscillates in a more regular fashion, with an amplitude of the order of 20% and a frequency which is approximately twice the value of the $\omega = 0$ case. The oscillations in the magnetic moment are larger, with spikes of 10% or more at approximately the same time as the minima of P_ϕ. It is clear that the interaction with the electric field produced by the rotation of the mode produces large changes in the energy, P_ϕ, and μ and that these changes are correlated with the large displacements shown in the particle orbit and the changes from trapped to passing. For the 18 keV trapped particle, the changes are smaller, both for $\omega = 0$ and $\omega \neq 0$, but the general trend is similar.

Considering now the 1 MeV particles, we see again that for $\omega = 0$, the changes are generally much smaller than for $\omega \neq 0$. The only exception is the P_ϕ of the counter passing particles, where the amplitude of the oscillations for $\omega = 0$ is approximately half the value for $\omega \neq 0$. Another important point is that due to the larger energy, the oscillations of μ in the unperturbed case are noticeable. In this case, the energy oscillations of the counter passing particle are smaller and more regular than for the trapped particle. Unlike the 18 keV case, the particles do not change their status, from passing to trapped or viceversa, and this explains why the temporal evolution of E, P_ϕ, and μ is clearly different. Note that although the relative energy changes are smaller, the absolute energy changes are actually larger for the 1 MeV particles. This can be explained by considering that the rate of change of the energy is $\mathbf{F} \cdot \boldsymbol{v}$, where $\mathbf{F}$ is the force acting on the particle and its velocity. Since the perturbation is the same in both cases, the rate of change of the energy depends on v ($\sim\sqrt{E}$) and $\boldsymbol{v}$ the phase. If the average phases were the same, the energy change should therefore increase as $\sqrt{E}$.

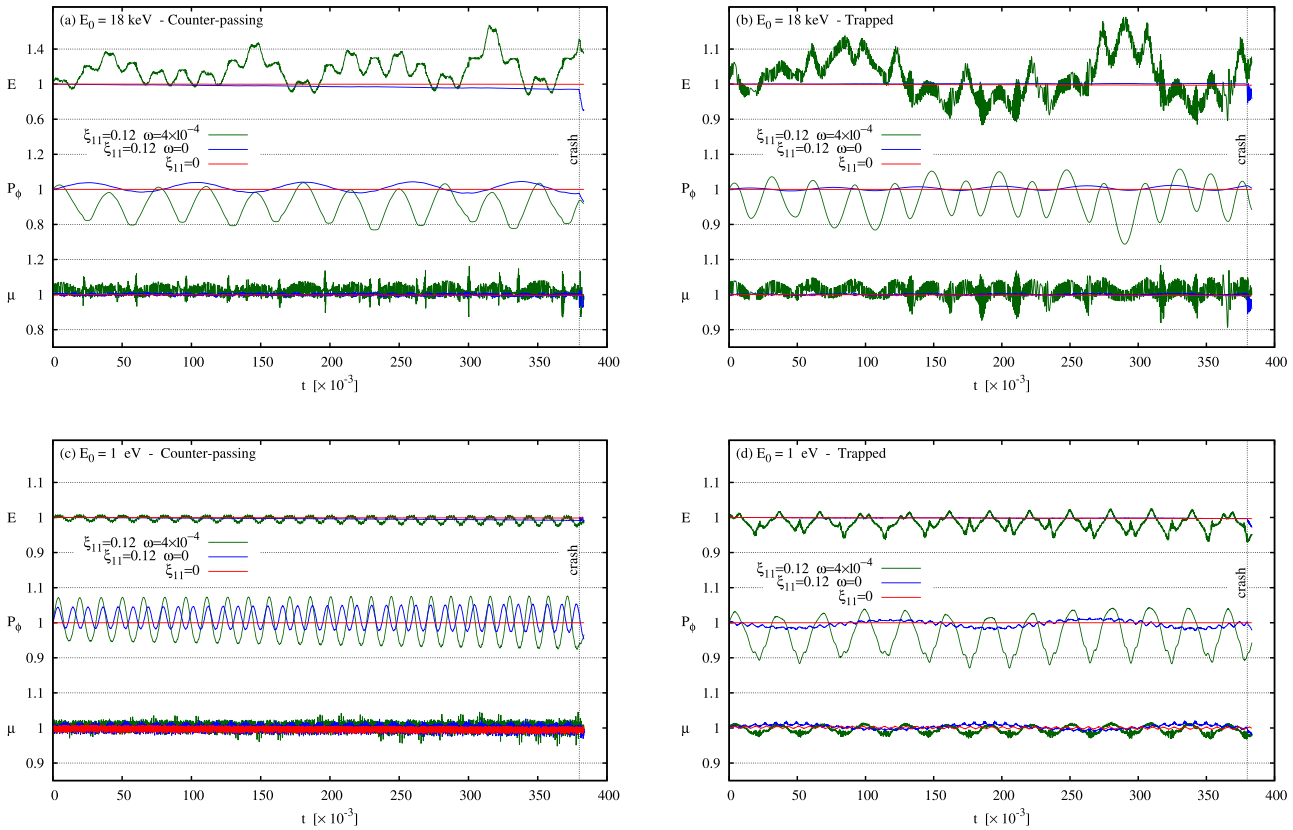

FIG. 18. Temporal variation of the energy, the toroidal component of the canonical momentum, and the magnetic moment for trapped and counter passing particles.

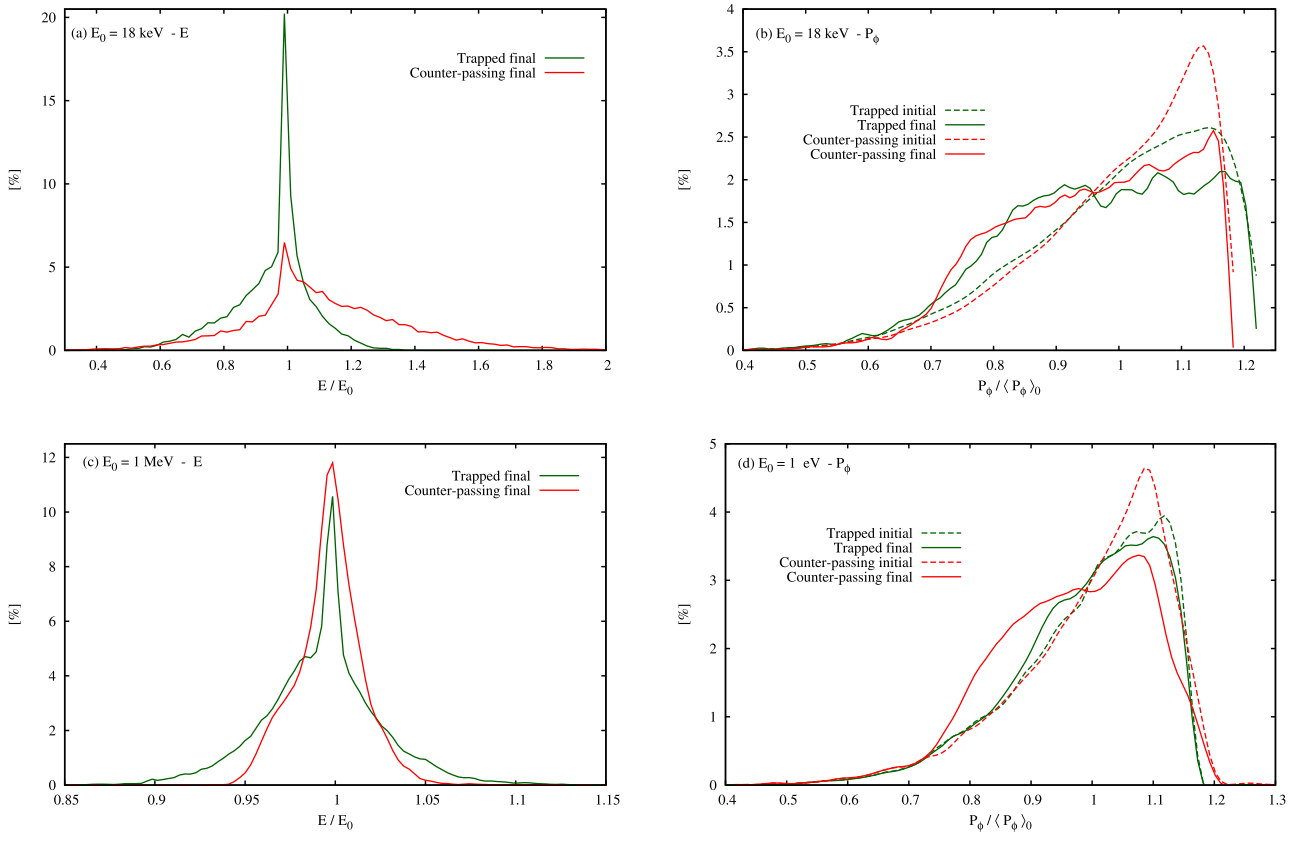

FIG. 19. Initial and final distributions of energy and P_ϕ for trapped and counter passing particles.

The results presented above concern a single particle of each type. Since it is clear that E, P_ϕ, and μ, oscillate (for $\omega \neq 0$) their final value will depend on the initial phase. That is, particles starting at different positions will have different final values of E, P_ϕ, and μ. To show what happens with a large number of particles, we present in Fig. 19 the initial and final distributions of E and P_ϕ obtained from a simulation with 50 000 particles. In these plots, the vertical axis indicates the percentage of particles having a given value of the quantity in the horizontal axis. Since each run contains particles having a given energy value, different initial positions and random pitch, the initial energy distribution is a δ function but the distribution of P_ϕ has a certain width. The horizontal energy axis has been normalized with the initial value, while the P_ϕ axis has been normalized with the average of the initial distribution.

Figure 19(a) shows that initially counter passing particles of 18 keV can finish the simulation with energies between 0.3 and 2 times their initial value and that the fraction of particles that have a final energy equal to the initial is very small. This is consistent with the large redistribution of 18 keV counter passing particles shown in Fig. 2. We remind that, in addition, these particles can change their status many times during the simulation. Trapped particles show a smaller energy spreading, with a larger fraction retaining their initial value. Figure 19(b) shows that the distribution of P_ϕ also spreads due to the perturbation. For both types of particles, the final distribution is broader and the initial maxima almost disappear. Again, the spreading is larger for the counter passing particles. Figures 19(c) and 19(d) show a similar behavior, except that the energy spreading is larger for trapped particles. Note that a 3% change in the energy of a 1 MeV particle is 30 keV, while a 30% change in the energy of an 18 keV particle is 5.4 keV, so the $\Delta E \sim \sqrt{E}$ relationship is approximately satisfied.

In summary, the results presented in this appendix show that even a relatively small amplitude, single mode perturbation can produce very large changes in the particle orbits. These changes occur because the perturbation destroys the constants of motion thus allowing the particles to move to different flux surfaces and also change from trapped to circulating or viceversa. Larger mode amplitudes and/or additional modes produce even larger changes.

[1]F. B. Marcus, J. M. Adams, A. D. Cheetham, S. Conroy, W. G. F. Core, O. N. Jarvis, M. J. Loughlin, M. Olsson, G. Sadler, P. Smeulders, P. Van Belle, and N. Watkins, Plasma Phys. Controlled Fusion **33**, 277 (1991).
[2]B. C. Stratton, R. J. Fonck, G. R. McKee, R. V. Budny, Z. Chang, F. Wising, and A. Odblom, Nucl. Fusion **36**, 1586 (1996).
[3]S. Nielsen, H. Bindslev, M. Salewski, A. Bürger, E. Delabie, V. Furtula, M. Kantor, S. B. Korsholm, F. Leipold, F. Meo *et al.*, Plasma Phys. Controlled Fusion **52**, 092001 (2010).
[4]C. M. Muscatello, W. W. Heidbrink, Y. I. Kolesnichenko, V. V. Lutsenko, M. A. Van Zeeland, and Yu. V. Yakovenko, Plasma Phys. Controlled Fusion **54**, 025006 (2012).
[5]M. F. F. Nave, J. Rapp, T. Bolzonella, R. Dux, M. J. Mantsinen, R. Budny, P. Dumortier, M. von Hellermann, S. Jachmich, H. R. Koslowski *et al.*, Nucl. Fusion **43**, 1204 (2003).
[6]Y. I. Kolesnichenko and Y. V. Yakovenko, Nucl. Fusion **36**, 159 (1996).
[7]Y. I. Kolesnichenko, V. V. Lutsenko, R. B. White, and Y. V. Yakovenko, Nucl. Fusion **40**, 1325 (2000).
[8]Y. I. Kolesnichenko, V. V. Lutsenko, R. B. White, and Y. V. Yakovenko, Phys. Lett. A **287**, 131 (2001).
[9]Y. Zhao and R. B. White, Phys. Plasmas **4**, 1103 (1997).
[10]R. Farengo, H. E. Ferrari, M.-C. Firpo, P. L. García-Martínez, and A. F. Lifschitz, Plasma Phys. Controlled Fusion **54**, 025007 (2012).
[11]R. Farengo, H. E. Ferrari, P. L. García-Martínez, M.-C. Firpo, W. Ettoumi, and A. F. Lifschitz, Nucl. Fusion **53**, 043012 (2013).
[12]V. Igochine, O. Dumbrajs, H. Zohm, A. Flaws, and ASDEX Team, Nucl. Fusion **47**, 23 (2007).
[13]R. B. White, *The Theory of Toroidally Confined Plasmas*, 2nd ed. (Imperial College Press, 2001), Chap. 7.
[14]I. T. Chapman, Plasma Phys. Controlled Fusion **53**, 013001 (2011).
[15]J. P. Graves, R. J. Hastie, and K. I. Hopcraft, Plasma Phys. Controlled Fusion **42**, 1049 (2000).